Title

Complement modulation in the retinal pigment epithelium rescues photoreceptor degeneration in a mouse model of Stargardt disease

Journal

Proceedings of the National Academy of Sciences of the United States of America, 114(15)

ISSN

0027-8424

Authors

Lenis, Tamara L
Sarfare, Shanta
Jiang, Zhichun
et al.

Publication Date

2017-04-11

DOI

10.1073/pnas.1620299114

Peer reviewed

Complement modulation in the retinal pigment epithelium rescues photoreceptor degeneration in a mouse model of Stargardt disease

Tamara L. Lenis[a,b,1], Shanta Sarfare[a,b,1,2], Zhichun Jiang[a,b], Marcia B. Lloyd[a,b], Dean Bok[a,b], and Roxana A. Radu[a,b,3]

[a]Stein Eye Institute, David Geffen School of Medicine, University of California, Los Angeles, CA 90095; and [b]Department of Ophthalmology, David Geffen School of Medicine, University of California, Los Angeles, CA 90095

Edited by Jeremy Nathans, Johns Hopkins University, Baltimore, MD, and approved March 3, 2017 (received for review December 9, 2016)

Recessive Stargardt macular degeneration (STGD1) is caused by mutations in the gene for the ABCA4 transporter in photoreceptor outer segments. STGD1 patients and *Abca4*$^{-/-}$ (STGD1) mice exhibit buildup of bisretinoid-containing lipofuscin pigments in the retinal pigment epithelium (RPE), increased oxidative stress, augmented complement activation and slow degeneration of photoreceptors. A reduction in complement negative regulatory proteins (CRPs), possibly owing to bisretinoid accumulation, may be responsible for the increased complement activation seen on the RPE of STGD1 mice. CRPs prevent attack on host cells by the complement system, and complement receptor 1-like protein y (CRRY) is an important CRP in mice. Here we attempted to rescue the phenotype in STGD1 mice by increasing expression of CRRY in the RPE using a gene therapy approach. We injected recombinant adeno-associated virus containing the CRRY coding sequence (AAV-CRRY) into the subretinal space of 4-wk-old *Abca4*$^{-/-}$ mice. This resulted in sustained, several-fold increased expression of CRRY in the RPE, which significantly reduced the complement factors C3/C3b in the RPE. Unexpectedly, AAV-CRRY–treated STGD1 mice also showed reduced accumulation of bisretinoids compared with sham-injected STGD1 control mice. Furthermore, we observed slower photoreceptor degeneration and increased visual chromophore in 1-y-old AAV-CRRY–treated STGD1 mice. Rescue of the STGD1 phenotype by AAV-CRRY gene therapy suggests that complement attack on the RPE is an important etiologic factor in STGD1. Modulation of the complement system by locally increasing CRP expression using targeted gene therapy represents a potential treatment strategy for STGD1 and other retinopathies associated with complement dysregulation.

recessive Stargardt macular degeneration | complement system | retinal pigment epithelium | bisretinoids | gene therapy

Recessive Stargardt macular degeneration (STGD1) is a blinding disease of children and young adults caused by mutations in the ATP binding cassette subfamily A member 4 (*ABCA4*) gene (1, 2). The pathological hallmark of STGD1 is deposition of autofluorescent lipofuscin in the retinal pigment epithelium (RPE), which precedes photoreceptor degeneration (3, 4). The exact mechanism of how RPE lipofuscin accumulation disrupts overall RPE performance is poorly understood. The RPE fulfills several photoreceptor support tasks, including phagocytosis of distal outer segments (OS) and processing of visual retinoids (5–8). In addition, the RPE plays a major role in controlling the ocular immune response through expression of various complement negative regulatory proteins (CRPs) (9). For these reasons, photoreceptors are critically dependent on a healthy RPE for continued viability.

The ABCA4 transporter clears retinaldehyde released by photobleached rhodopsin and cone-opsins from OS discs in the form of *N*-retinylidene phosphatidylethanolamine (*N*-ret-PE) (10). As a result, mice lacking ABCA4 accumulate retinaldehyde and *N*-ret-PE in their OS after light exposure (11), which promotes condensation of *N*-ret-PE with a second retinaldehyde to yield a series of bisretinoid pigments that build up as lipofuscin in the RPE with advancing age (12–15). This accumulation is greatly enhanced in the RPE of STGD1 patients and *Abca4*$^{-/-}$ mice (STGD1) (16). Fluorescent bisretinoid-lipofuscin pigments can be visualized by fundus autofluorescence imaging (17, 18) and are responsible for the "dark choroid" seen in STGD1 patients on fluorescein angiography (19). One of the major lipofuscin components in the RPE of *Abca4*$^{-/-}$ mice and STGD1 patients is *N*-retinylidene-*N*-retinylethanolamine (A2E) (15). A2E and other bisretinoids exhibit several mechanisms of cytotoxicity (20–23) and are thought to contribute to STGD1 pathogenesis (24). Importantly, bisretinoids and their oxidation products have been shown to activate complement in cultured RPE cells (25, 26). Increased inflammatory markers and complement activation also have been observed in *Abca4*$^{-/-}$ mice (27). Degeneration of photoreceptors in these animals has been attributed to degraded RPE function owing to chronic bisretinoid-mediated complement dysregulation (27, 28).

Age-related macular degeneration (AMD), a disease with significant similarities to STGD1, is also associated with RPE lipofuscin accumulation and complement dysregulation (29). The genes for multiple proteins of the complement cascade, such as complement factor H (*CFH*), are susceptibility loci for AMD (30–32). CFH is a soluble CRP secreted by liver and RPE cells (33). Notably, complement activation in bisretinoid-laden RPE cells has been shown to be strongly dependent on the *CFH* haplotype (34). Moreover, a subset of AMD has been linked to *ABCA4* mutations, suggesting a

Significance

The complement system, a key component of innate immunity, is necessary to maintain tissue homeostasis. In the eye, the retinal pigment epithelium (RPE) plays a major role in controlling the immune response through expression of various complement negative regulatory proteins (CRPs). Here we identify that inappropriate activation of the complement cascade plays a role in the pathogenesis of recessive Stargardt disease (STGD1). Using the STGD1 mouse model, we show that overexpression of the complement receptor 1-like protein y, a major murine CRP, reduces complement attack on the RPE and rescues both bisretinoid accumulation and photoreceptor degeneration. Our data demonstrate that STGD1 presents with dysregulation of the complement system as also has been proposed for age-related macular degeneration, supporting a common etiologic pathway.

Author contributions: T.L.L., S.S., and R.A.R. designed research; T.L.L., S.S., Z.J., M.B.L., and R.A.R. performed research; T.L.L., S.S., M.B.L., D.B., and R.A.R. analyzed data; and T.L.L., S.S., and R.A.R. wrote the paper.

The authors declare no conflict of interest.

This article is a PNAS Direct Submission.

Freely available online through the PNAS open access option.

[1]T.L.L. and S.S. contributed equally to this work.

[2]Present address: Department of Biomedical Science and Disease, New England College of Optometry, Boston, MA 02115.

[3]To whom correspondence should be addressed. Email: radu@jsei.ucla.edu.

This article contains supporting information online at www.pnas.org/lookup/suppl/doi:10.1073/pnas.1620299114/-/DCSupplemental.

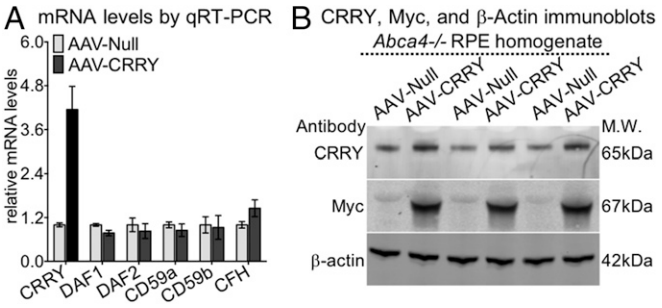

Fig. 1. Increased expression of CRRY in the RPE cells by subretinal injection of AAV-CRRY. (*A*) Histogram showing relative CRRY, DAF1, DAF2, CD59a, CD59b, and CFH mRNA levels by qRT-PCR. Each mRNA level was normalized to 18S rRNA. (*B*) Representative immunoblot of CRRY (65-kDa isoform), Myc, and β-actin using RPE homogenate (10 μg of protein per lane). Protein and cDNA samples were obtained from 1-y-old *Abca4*$^{-/-}$ mice injected with AAV-CRRY and -null viruses. Data represent mean ± SD; $n = 5$ mice. Each protein and cDNA sample was run in triplicate. M.W., molecular weight.

convergent pathogenesis for STGD1 and AMD (35). Although effective treatments exist to temporize the "wet" form of AMD associated with choroidal neovascularization (36–39), no effective treatments exist for the early "dry" form of AMD that more closely resembles STGD1.

To date, the contribution of complement dysregulation to the pathogenesis of STGD1 has not been assessed in live animals. In the present study, we attempted to normalize complement activity in the eye by increasing expression of complement receptor 1-like protein y (CRRY) in the *Abca4*$^{-/-}$ RPE cells. To this end, we injected recombinant adeno-associated virus containing the gene for CRRY (AAV-CRRY) into the subretinal space of STGD1 mice. We assessed complement reactivity, bisretinoid accumulation, oxidative stress, photoreceptor morphology, and physiological responses of the retina up to 1 y following delivery of the virus.

Results

AAV-CRRY Subretinal Injection Results in Increased Expression of CRRY in the RPE Cells. Subretinal delivery of 13,000 multiplicity of infection (MOI) AAV-CRRY or AAV-null virus in 0.5 μL of injection volume was performed under direct visualization and confirmed by fundus imaging and optical coherence tomography (OCT) in 4-wk-old mice. The CRRY construct was designed with a Myc tag, allowing us to distinguish the AAV-expressed protein from endogenous CRRY. We confirmed expression of Myc-tagged CRRY protein in RPE homogenates of *Abca4*$^{-/-}$ mice by immunoblotting at 5 wk after subretinal injection. In AAV-CRRY RPE homogenates, the protein was detected by both CRRY and Myc antibodies, whereas RPE homogenates from uninjected and null-injected (AAV-GFP) *Abca4*$^{-/-}$ mice exhibited reactivity only with the CRRY antibody (Fig. S1*B*); however, Myc immunoreactivity was undetectable in the neural retina homogenates, suggesting RPE specificity (Fig. S1*C*). CRRY mRNA expression was measured by quantitative RT-PCR (qRT-PCR) using cDNA from mouse RPE as the template. By 1 y postinjection, the CRRY mRNA was fourfold more abundant in AAV-CRRY–injected vs. AAV-null–injected *Abca4*$^{-/-}$ mice (Fig. 1*A*). Consistently, levels of recombinant CRRY were higher in RPE homogenates from AAV-CRRY–injected vs. AAV-null–injected mice by immunoblotting, using antibodies against CRRY and Myc (Fig. 1*B*). These results indicate stable long-term expression of AAV-CRRY. Expression of other CRP mRNAs was not significantly altered in the RPE of AAV-CRRY–injected *Abca4*$^{-/-}$ mice (Fig. 1*A*).

CRRY overexpression correlates with decreased accumulation of complement C3 and its breakdown fragments in the RPE. Complement factor C3 is cleaved to generate the C3bBb convertase, C3b, and its breakdown fragment (iC3b) on initiation of the complement cascade. To determine whether overexpression of CRRY results in decreased C3 convertase, we evaluated C3/C3b levels in the eyes of injected animals by immunohistochemistry and quantitative immunoblotting. C3/C3b (red) immunofluorescence was reduced in RPE sections from AAV-CRRY–injected vs. AAV-null–injected mice (Fig. 2*A*). In these animals, CRRY overexpression was confined to the RPE by Myc (green) immunofluorescence (Fig. 2*A*). To confirm this finding, we measured C3 in RPE homogenates by quantitative immunoblotting. At 1 y of age, C3/C3b levels were twofold lower in AAV-CRRY–injected vs. AAV-null–injected mice (Fig. 2*B*). These results suggest that overexpression of CRRY reduced complement activation on the RPE, as intended.

RPE autofluorescence is decreased in the AAV-CRRY–injected* Abca4$^{-/-}$ *mice. Accumulation of autofluorescent bisretinoids in the RPE is a hallmark of STGD1 (15). It was previously shown that C3 breakdown fragments become internalized in the RPE cells of *Abca4*$^{-/-}$ mice and colocalize with endogenous autofluorescence (27). We investigated the distribution of CRRY by immunofluorescence and the distribution of autofluorescent bisretinoids in RPE flat mounts from 6-mo-old *Abca4*$^{-/-}$ mice. Age-matched wild-type (BALB/c) mice exhibited lower autofluorescence compared with AAV-null–injected *Abca4*$^{-/-}$ mice, as anticipated (Fig. 3). AAV-CRRY–injected *Abca4*$^{-/-}$ mice exhibited significantly lower autofluorescence (green) in the RPE compared with AAV-null–injected *Abca4*$^{-/-}$ mice (Fig. 3). Only the AAV-CRRY–injected mice showed significant Myc immunofluorescence in the RPE (red) (Fig. 3). Subretinal injection of the virus in the superior-temporal region covered only approximately one-third of the retina; the flat mounts in Fig. 3 are from this treated area. As expected, RPE from an inferior-nasal region remote from the superior-temporal site of injection exhibited minimal Myc immunofluorescence (Fig. S2, away from the injection site). In addition, RPE autofluorescence was higher in this nonrescued region (Fig. S2), suggesting a correlation between CRRY overexpression and reduced bisretinoid accumulation in the RPE of *Abca4*$^{-/-}$ mice.

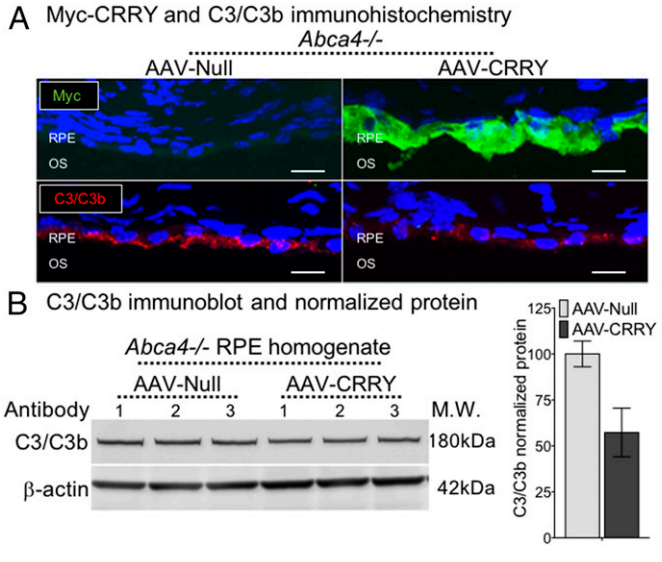

Fig. 2. Reduced C3/C3b immunoreactivity in AAV-CRRY–treated *Abca4*$^{-/-}$ mice. (*A*) Representative confocal images of Myc (green), C3/C3b (red), and DAPI (blue) immunohistochemistry in 5-mo-old *Abca4*$^{-/-}$ mice injected with AAV-CRRY and -null viruses ($n = 3$ mice). Images were taken from the superior-temporal quadrant. (Scale bar: 10 μm.) (*B*) Representative immunoblot of C3/C3b and β-actin using RPE homogenate (10 μg protein per lane). C3/C3b band intensity in RPE homogenate samples was normalized to β-actin. Data in the histogram are mean ± SD; $n = 6$ mice. $P < 0.005$. Note the approximate twofold reduction in C3/C3b levels in the AAV-CRRY group.

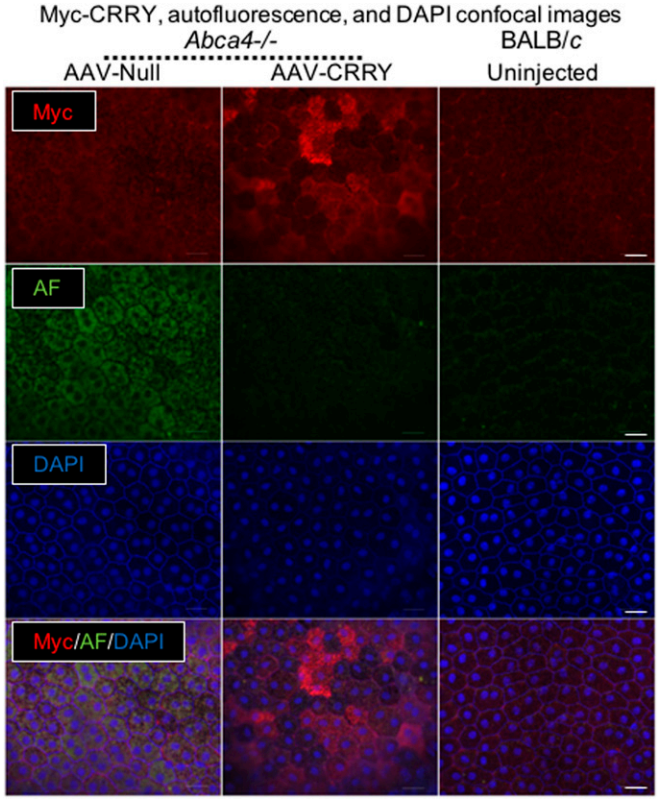

Fig. 3. Decreased RPE autofluorescence in AAV-CRRY–injected *Abca4*$^{-/-}$ mice. Representative confocal images of Myc (red) and DAPI (blue) immunohistochemistry; autofluorescence (AF, green) acquired at an 488-nm excitation wavelength in 6-mo-old *Abca4*$^{-/-}$ mice injected with AAV-CRRY and -null viruses (*Left* and *Middle*) and age-matched untreated BALB/c mice (*Right*). Images were taken from the superior-temporal quadrant. Autofluorescence intensity inversely correlates with levels of Myc-CRRY expression in the *Abca4*$^{-/-}$ mice (n = 4). (Scale bar: 20 μm.)

Bisretinoid levels are reduced in AAV-CRRY–injected* Abca4$^{-/-}$ *mice. We quantified bisretinoids by liquid chromatography in wild-type and *Abca4*$^{-/-}$ RPE at 11–12 mo postinjection. Both A2PE-H_2 and A2E were ∼2.5-fold reduced in *Abca4*$^{-/-}$ mice that received the AAV-CRRY virus vs. those that received the AAV-null virus (Fig. 4). Still lower levels of bisretinoids were present in noninjected, age-matched wild-type mice (Fig. 4).

CRRY overexpression did not affect oxidative stress or autophagy in* Abca4$^{-/-}$ *RPE. Bisretinoid accumulation in the RPE is partly responsible for inducing cellular oxidative stress and compromised autophagy (27, 40). We measured mRNA and protein expression of superoxide dismutase-1 (SOD-1) along with a mitochondria-specific marker, superoxide dismutase-2 (SOD-2), in the eyes of 7-mo-old AAV-CRRY– and AAV-null–injected mice by qRT-PCR and immunoblotting (Fig. S3). SOD-1 and SOD-2 mRNA and protein were present at similar levels in the RPE cells of AAV-CRRY–injected and AAV-null–injected mice (Fig. S3).

We also measured the lipidated form of microtubule-associated protein light chain 3 (LC3) in the RPE of wild-type and *Abca4*$^{-/-}$ mice at 6 mo after subretinal injection of AAV-CRRY or AAV-null virus. We observed a significant decrease in LC3 levels in RPE homogenates from *Abca4*$^{-/-}$ mice vs. age-matched wild-type mice; however, LC3 immunoreactivity was not influenced by CRRY overexpression in either the wild-type or the *Abca4*$^{-/-}$ RPE (Fig. S4). Thus, oxidative stress and impaired autophagy might not be improved by increasing CRRY expression.

Lipofuscin deposition in RPE cells is decreased after AAV-CRRY injection. Accumulation of lipofuscin granules in the RPE occurs with normal aging and is greatly accelerated in *Abca4*$^{-/-}$ mice (11, 41). Electron microscopy analysis of retinal sections of AAV-CRRY–injected *Abca4*$^{-/-}$ eyes showed significantly reduced pigment granules in the RPE cells compared with AAV-null–injected *Abca4*$^{-/-}$ eyes (Fig. 5*A*). To quantify these lipofuscin pigments, we measured the RPE cell area occupied with pigment granules divided by the total cytoplasmic area. The fractional area of lipofuscin granules in the RPE was ∼30% lower in AAV-CRRY–injected *Abca4*$^{-/-}$ eyes compared with AAV-null–injected *Abca4*$^{-/-}$ eyes; however, AAV-CRRY– and AAV-null–injected *Abca4*$^{-/-}$ eyes showed 2.5-fold and 1.8-fold, respectively, higher lipofuscin deposition compared with uninjected wild-type eyes (Fig. 5*B*).

Overexpression of CRRY in the RPE protects* Abca4$^{-/-}$ *photoreceptors from degeneration. Albino *Abca4*$^{-/-}$ mice exhibit slow degeneration of photoreceptors (16). Here we tested whether overexpression of CRRY in the RPE of *Abca4*$^{-/-}$ mice had a protective effect. We performed light microscopy (LM) on fixed retinal sections from regions overlying the site of virus injection from ∼1-y-old mice. AAV-CRRY–injected *Abca4*$^{-/-}$ mice exhibited significantly more photoreceptor nuclei in the outer nuclear layer (ONL) compared with AAV-null–injected *Abca4*$^{-/-}$ mice (Fig. 6 *A* and *B*). In the rescued area, the number of ONL nuclei were similar in AAV-CRRY–injected *Abca4*$^{-/-}$ mice and wild-type mice (Fig. 6 *A* and *B*). These results suggest nearly complete protection from photoreceptor degeneration in the injected region (superior-temporal).

To confirm these findings, we measured levels of 11-*cis*-retinaldehyde (11-*cis*-RAL) chromophore in dark-adapted mice, which correlates with the number of rhodopsin molecules. At ∼11 mo postinjection, AAV-CRRY–injected *Abca4*$^{-/-}$ whole eyes contained 25% more 11-*cis*-RAL than AAV-null–injected *Abca4*$^{-/-}$ whole eyes (Fig. 7). Still higher levels of 11-*cis*-RAL were present in age-matched wild-type control mice (Fig. 7). The less dramatic rescue of photoreceptor degeneration by 11-*cis*-RAL levels likely reflects the averaging of protected and nonprotected areas in the AAV-CRRY–injected mice.

Discussion

Accumulation of bisretinoid pigments in the RPE of *Abca4*$^{-/-}$ mice causes significant complement dysregulation that further contributes to RPE dysfunction and subsequent photoreceptor degeneration (15, 16, 27). In this study, we attempted to protect cells against complement attack by increasing expression of CRRY in the RPE of *Abca4*$^{-/-}$ mice. CRRY is an important CRP in the mouse eye (9). The functional human homolog of CRRY is Membrane Cofactor Protein (MCP, or CD46), which is implicated in several human inflammatory diseases, including AMD (42, 43). A single subretinal injection of AAV-CRRY in 4-wk-old *Abca4*$^{-/-}$ mice was sufficient to sustain a several-fold increase in CRRY expression in the RPE beyond 1 y without affecting the levels of other CRPs (Fig. 1). CRRY prevents cleavage of complement components C3 and C5, which generate reactive breakdown

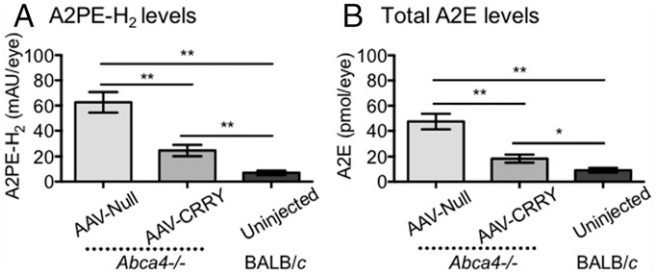

Fig. 4. Reduced bisretinoid levels in AAV-CRRY–injected *Abca4*$^{-/-}$ mice. Bisretinoids were quantified by HPLC from chloroform extracts of a single eye from 1-y-old *Abca4*$^{-/-}$ and BALB/*c* mice. A2PE-H_2 (*A*) and A2E (*B*) are expressed as milliabsorbance units (mAU) and picomoles (pmol) per eye, respectively. Data represent mean ± SD; n = 6–8 mice. *P < 0.05; **P < 0.005.

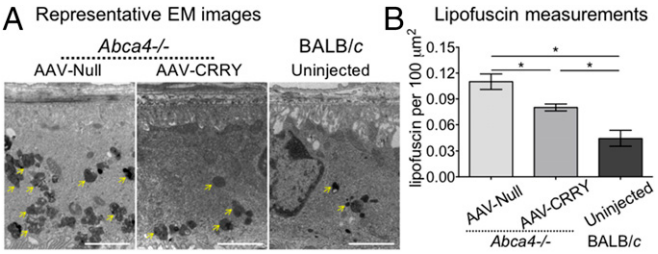

Fig. 5. Lipofuscin accumulation is decreased in CRRY-injected *Abca4*$^{-/-}$ mice. (*A*) Representative EM images of RPE from 1-y-old *Abca4*$^{-/-}$ and BALB/*c* mice. Arrows indicate electron-dense lipofuscin granules. (Scale bar: 2 μm.) (*B*) Histogram showing the lipofuscin fractional area measurements by EM. Images were taken from the superior nasal quadrant. Data are presented as mean ± SD; $n = 4$–11 mice. *$P < 0.005$.

fragments that form the cytolytic membrane attack complex (MAC) (44). These proteins can deposit on the plasma membrane of RPE cells to create a sublytic complex that degrades RPE function without killing the cell (45, 46). CD46 is expressed in the basolateral membranes of human RPE cells, where it is exposed to the choroidal circulation. CD46 and CRRY bind complement C3b with high affinity, inhibiting the C3 convertase amplification loop that leads to MAC deposition (47). Here we have shown that CRRY overexpression in AAV-CRRY–injected *Abca4*$^{-/-}$ eyes leads to reduced deposition of the C3 breakdown fragments C3b and iC3b (Fig. 2).

The presence of reactive complement proteins on the surface of RPE cells may accelerate lipofuscin accumulation by impeding its clearance via endolysosomes within the RPE (48). This concept is supported by the observation that the RPE region transduced by the AAV-CRRY virus exhibited decreased autofluorescence (Fig. 3). In the case of STGD1 patients and *Abca4*$^{-/-}$ mice, this autofluorescent material contains abundant A2E and related bisretinoids (15, 49). Bisretinoid levels in the AAV-CRRY–injected mice were approximately twofold lower than those in the AAV-null–injected mice (Fig. 4). These data lend further support to the association between complement activation and buildup of vitamin A byproducts in RPE cells. Increased bisretinoid-lipofuscin granules within RPE cells have been shown to inhibit cholesterol-mediated autophagy (40). We measured levels of LC3, a key marker of autophagy, in response to AAV-CRRY injection. Although the relative amount of LC3 was significantly lower in the *Abca4*$^{-/-}$ mice compared with the wild-type mice, similar levels of LC3 were observed in mice that received AAV-CRRY virus injections and those that received AAV-null virus injections (Fig. S4). Likewise, antioxidative stress protein levels were similar in the AAV-CRRY–injected and AAV-null–injected *Abca4*$^{-/-}$ mice (Fig. S3). These data suggest that even mild accumulations of bisretinoid-lipofuscin above the levels in wild-type mice are sufficient to induce cellular stress.

A major effect of increasing CRRY expression in the RPE of the *Abca4*$^{-/-}$ mice was the slowing of photoreceptor degeneration (Fig. 6). We observed an ∼30% increase in the number of photoreceptor nuclei in the area transduced by the AAV-CRRY treatment. This modest but significant rescue was evidenced by increased visual chromophore in AAV-CRRY–treated *Abca4*$^{-/-}$ mice (Fig. 7). In *Abca4*$^{-/-}$ mice and STGD1 patients, photoreceptor degeneration is attributed to bisretinoid accumulation by the RPE (4, 15). With time, the combination of bisretinoid accumulation and complement activation may impair the recycling of retinoids released from phagocytosed OS in the RPE. This favors the formation of bisretinoids, such as A2E (8). Reduced bisretinoid levels have been observed in *Abca4*$^{-/-}$ mice treated with drugs that lower circulating vitamin A or inhibit enzymes of the visual cycle (28, 41, 50). Combination drug therapy with both complement modulators and visual cycle inhibitors may be an effective treatment strategy for STGD1 because it targets both pathogenic mechanisms.

Rescue of both bisretinoid accumulation and photoreceptor degeneration by subretinal injection of AAV-CRRY suggests that inappropriate activation of the complement cascade plays a role in the pathogenesis of STGD1. Correlation between monoallelic sequence variants in the *ABCA4* gene and a clinically distinct subset of "dry" AMD patients (51), together with the present findings, suggest a common final etiologic pathway for STGD1 and some cases of AMD (51). In AMD, complement dysfunction in the RPE can be caused by mutations in the gene for CFH or other complement regulatory proteins (52–55). In contrast, the primary defect in STGD1 is lack of the functional ABCA4 transporter, which is responsible for the formation and accumulation of toxic bisretinoids in the RPE (2, 15). Degeneration of macular photoreceptors in both diseases results from loss of RPE support. Our study shows that normalizing local complement activity in aged or diseased RPE may prolong photoreceptor viability.

Materials and Methods

Animals. Albino *Abca4*$^{-/-}$ and BALB/*c* mice were housed in 12-h light/12-h dark conditions and fed ad libitum. Mice were on the homozygous Leu450 Rpe65 variant and free of Rd8 mutations. All experiments were performed in accordance with the Association for Research in Vision and Ophthalmology statement and University of California Institutional Animal Care and Use Committee guidelines for animal care and approved research protocols.

Generation of Adeno-Associated Viral Vector Expressing CRRY. The murine CRRY gene was amplified by PCR from a cDNA clone (Origene NM_013499) (56). A carboxy terminal c-Myc tag was added using oligonucleotides (forward: 5′-CACACACGCTAGCCCTCTTAAAAGATCCAAAAAATGAGACTTCTAGC-3′; reverse: 5′-TGTGTGCTCGAGTTACAGATCCTCTTCTGAGATGAGTTTTTGTTCGGAGACTTCTTGAGTGAGTGAATTCCGTG-3′) and subcloned into pAAV8-CAG-MCS (Vector Biolabs) within restriction sites XhoI to NheI to generate pAAV8-CAG-CRRY-Myc (CRRY-Myc) (Fig. S1*A*). The construct was verified with restriction digests and by sequencing analysis. The CRRY-Myc construct was packaged in an AAV2 vector genome pseudoserotyped with the type 8 capsid (AAV-CRRY) by the Penn Vector Core (57). Control vectors, such as AAV2/8 null (AAV-null) and a vector expressing green-fluorescence protein (AAV-GFP), were obtained from SignaGen Laboratories.

Subretinal Injections. Mouse eyes were dilated with 2.5% phenylephrine (Hub Pharmaceuticals) and 0.5% tropicamide (Akorn Pharmaceuticals). Mice were anesthetized with 100 mg/kg ketamine (Phoenix Pharmaceuticals) and 8 mg/kg xylazine (Lloyd Laboratories). Before injection, the AAV-CRRY, -GFP, and -null vector stock solutions were diluted from 2×10^{12} to 2×10^{13} GC/mL to deliver an MOI of ∼13,000 in a volume of 0.5 μL. A multipurpose 2.7-mm telescoping modified endoscope (Karl Storz) was used to perform the subretinal injections in the superior-temporal quadrant under direct visual control. The endoscope tip was illuminated via a fiber optic cable connected to a xenon light source and connected to a high-definition camera and Image 1 Hub monitor (Karl Storz). A superior-temporal scleral incision was made with a 33-gauge needle, followed by insertion of a blunt-tip 33-gauge needle on a Hamilton syringe. Successful injections were identified by OCT (Bioptigen) and fundus imaging

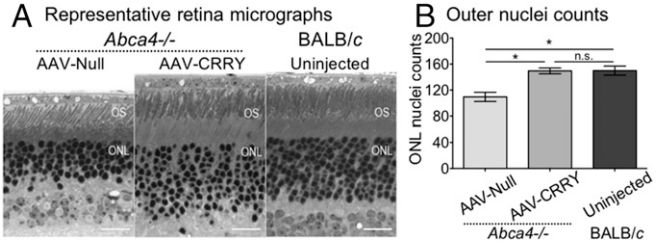

Fig. 6. Rescue of photoreceptor cells in CRRY-injected *Abca4*$^{-/-}$ mice. (*A*) Representative LM images of retinas from 1-y-old *Abca4*$^{-/-}$ and BALB/*c* mice. (Scale bar: 20 μm.) (*B*) Histogram showing the ONL nuclei counts by LM. Images were taken from the superior-temporal quadrant. Data are mean ± SD; $n = 5$–9 mice. *$P < 0.005$.

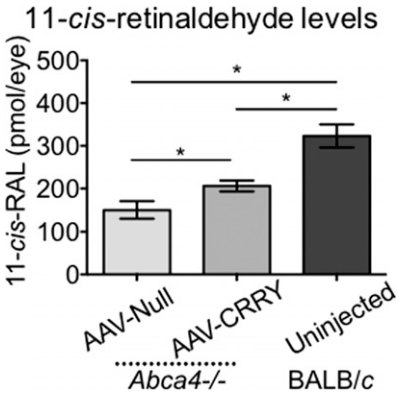

Fig. 7. Visual chromophore (11-*cis*-RAL) is increased in CRRY-injected *Abca4*$^{-/-}$ mice. Retinoid levels were quantified by HPLC from hexane extracts of a single eye from 1-y-old *Abca4*$^{-/-}$ and BALB/*c* mice. The 11-*cis*-RAL data are expressed as mean ± SD, in pmol per eye; $n = 6$–8 mice. *$P < 0.005$.

(Karl Storz) immediately after injection and at different time points thereafter. The mice were kept on a 37 °C heating pad during the subretinal injection, recovery after the anesthesia, and follow-up fundus examination. Eyes exhibiting evidence of retinal damage or hemorrhage by fundus visualization or OCT were excluded from further analysis.

qRT-PCR. Total RNA was extracted from mouse RPE homogenate using an Absolutely RNA Miniprep Kit (Stratagene) with DNase treatment and reverse-transcribed to cDNA using SuperScript III (Invitrogen) in accordance with the manufacturer's protocol. qRT-PCR was performed with SYBR Green (Invitrogen) and mouse gene-specific primer sets for CRRY, DAF1, DAF2, CD59a, CD59b, CFH, SOD-1, and SOD-2 following a previously reported protocol (27). RNA expression was normalized to 18S rRNA Ct values for each sample, and relative mRNA levels were recorded as mean ± SD ($n = 5$ eyes for each group).

Immunoblotting. RPE/eyecup vs. neural retina tissue from each animal was homogenized in 1× PBS with Halt protease inhibitor mixture (Life Technologies). Protein samples were treated with benzonase nuclease (Sigma-Aldrich) at room temperature for 1 h and then rehomogenized with 1% SDS. Cellular debris was removed using centrifugation, and protein concentration was determined using the Micro BCA Protein Assay Kit (Thermo Fisher Scientific). Proteins were then separated on 4–12% SDS/PAGE gels (Novex; Invitrogen) as described previously (27). Membranes were blocked with Odyssey Blocking Buffer (LI-COR Biosciences), followed by incubation at room temperature, and then probed with antibodies against Myc (c-myc; PA1-22826; Thermo Fisher Scientific), α-tubulin (T9026; Sigma-Aldrich), LC3 (L7543; Sigma-Aldrich), β-actin (A00702; Genscript), C3/C3b/iC3b (HM1065; Hycult Biotech), CRRY (sc-30214; Santa Cruz Biotechnology), SOD-1 (sc-11407; Santa Cruz Biotechnology), and SOD-2 (sc-30080; Santa Cruz Biotechnology). The predominant isoforms of recombinant CRRY detected by CRRY antibody were 53 kDa and 65 kDa; Myc immunostaining consistently confirmed recombinant CRRY expression. Western blot analysis was performed using cognate IR dye-labeled secondary antibodies and detected with an Odyssey CLx Infrared Imaging System (LI-COR).

Immunohistochemistry and Confocal Microscopy. Before enucleation, all eyes were marked by cauterization on the superior pole. The eyes were immersion-fixed in 4% paraformaldehyde for 2 h on ice for RPE-choroid-sclera flat mounts or overnight at 4 °C for frozen sections. For frozen sections, after fixation, the eyes were embedded in CRYO-OCT (Tissue-Tek) and cut into 10-μm sections for C3/C3b and Myc immunohistochemistry as described previously (27). For flat mounts, eyecups were dissected into eight leaflets, permeabilized with 1% Triton X-100, and blocked with 1% BSA/5% normal goat serum in 0.1 M $NaPO_4$ buffer (pH 7.0). RPE-choroid-sclera flat mounts were incubated overnight at 4°C with anti-rabbit ZO-1 (61-7300; Thermo Fisher Scientific) and anti-mouse c-myc (PA1-22826) and then stained with goat anti-rabbit Alexa Fluor 647 conjugate and anti-mouse Alexa Fluor 568 conjugate secondary antibodies for 1 h at room temperature. The RPE flat mounts (with apical RPE facing up) and retinal sections were mounted in Prolong Gold anti-fade reagent containing DAPI nuclear staining (Life Technologies) and imaged from the superior-temporal quadrant using a 60× oil-immersion lens with an Olympus Fluoview FV1000 confocal microscope. The RPE flat mounts were imaged at a single 3-μm-thick *z*-plane at the mid-RPE level. RPE autofluorescence was evaluated using an excitation wavelength of 488 nm and an emission wavelength of 500–545 nm.

Light and Electron Microscopy. Mice were euthanized under anesthesia and fixed by intracardiac perfusion with 2% formaldehyde and 2.5% glutaraldehyde in 0.1 M sodium phosphate buffer (pH 7.2). The nasal and temporal hemispheres of each eyecup were separated and also fixed in 1% osmium tetroxide dissolved with 0.1 M sodium phosphate, then dehydrated in a graded series of alcohols. The temporal hemispheres were embedded in a mixture of tEpon-812 (Tousimis Research) and Araldite (Electron Microscopy Sciences) for LM. Then 1-μm-thick sections stained with toluidine blue were imaged in the region of the injected quadrant (superior-temporal) with a 63× objective using a CoolSNAP digital camera (Photometrics) affixed to a Zeiss Axiophot microscope. The total number of photoreceptor nuclei in three independent areas in the region of the injection site (superior-temporal quadrant) were counted and plotted in PrismGraph program. Data are presented as mean ± SD (AAV-null–injected *Abca4*$^{-/-}$ mice, $n = 6$ eyes; AAV-CRRY–injected *Abca4*$^{-/-}$ mice, $n = 11$ eyes; uninjected BALB/*c* mice, $n = 4$ eyes).

The nasal hemispheres were cut into quadrants and embedded in Araldite 502 (Electron Microscope Sciences) for electron microscopy (EM). Ultrathin sections were cut on a Leica Ultracut microtome, collected on 200-mesh copper grids, and double-stained with uranium and lead salts. The ultrathin sections were imaged on a JEM 1200-EX electron microscope (JEOL). At least 10 100-μm^2 images were acquired from the superior-nasal quadrant of each eye at 15,000× magnification. Using OSIS software (EMSIS), fractional lipofuscin granules were measured by obtaining the area (in μm^2) occupied by lipofuscin over the area (in μm^2) occupied by cytoplasm. Each animal's fractional lipofuscin granule measurement corresponded to an average of at least 10 adjacent EM images from one eye ($n = 5$–9 animals per group).

Quantification of Retinoids and Bisretinoids. Retinoid and bisretinoid levels in the mouse whole eyes were determined using previously published methods (27, 58). Mice were dark-adapted overnight, and all tissue manipulations were performed under dim red light (Kodak Wratten 1A filter). Each eye was homogenized in 1× PBS, mixed with chloroform/methanol (2:1, vol/vol), and extracted with chloroform for bisretinoid analysis. For 11-*cis*-RAL quantification, a single eye homogenization was done in the presence of hydroxylamine and extracted in hexane. The organic phase was dried under an argon stream and resuspended in 100 μL of isopropanol and 100 μL of hexane. Absorption units corresponding to the A2E peak at 435 nm were converted to picomoles using a calibration curve with an authentic A2E standard and the published molar extinction coefficient for A2E (12). Eluted retinal oxime peaks were identified by spectra and elution time, and absorption units were converted to picomoles using a calibration curve based on authentic standards and published molar extinction coefficients (59).

Statistical Analysis. Data are presented as mean ± SD of a minimum of four to six animals per group unless specified otherwise. Two-group comparisons were performed using Student's *t*-test in Microsoft Excel, and multiple group comparisons were performed using ANOVA in JMP Pro v12 (SAS Institute).

ACKNOWLEDGMENTS. We thank Jeremy Cook and Gabriel Travis for their critical review of the manuscript; Fei Yu for his valuable assistance with the statistical analysis; and Anita Kim, Shannan Eddington, and Steven McMullen for their outstanding technical support. This study was supported by the National Eye Institute (Grants R01 EY025002, to R.A.R., and Stein Eye Institute Core Grant for Vision Research EY000331), an unrestricted grant from Research to Prevent Blindness, the BrightFocus Foundation (R.A.R.), the Macula Vision Research Foundation (R.A.R. and D.B.), the Gerald Oppenheimer Family Foundation Center for the Prevention of Eye Disease (R.A.R.), the Dolly Green Endowed Chair in Ophthalmology (D.B.), and a Sarkaria philanthropic award (to R.A.R.).

1. Lewis RA (1999) Dominant retinal dystrophies and Stargardt disease. *Ophthalmic Genet* 20:69–70.
2. Allikmets R (1997) A photoreceptor cell-specific ATP-binding transporter gene (ABCR) is mutated in recessive Stargardt macular dystrophy. *Nat Genet* 17:122.
3. Delori FC, et al. (1995) In vivo measurement of lipofuscin in Stargardt's disease–Fundus flavimaculatus. *Invest Ophthalmol Vis Sci* 36:2327–2331.
4. Cideciyan AV, et al. (2004) Mutations in ABCA4 result in accumulation of lipofuscin before slowing of the retinoid cycle: A reappraisal of the human disease sequence. *Hum Mol Genet* 13:525–534.
5. Flannery JG, O'Day W, Pfeffer BA, Horwitz J, Bok D (1990) Uptake, processing and release of retinoids by cultured human retinal pigment epithelium. *Exp Eye Res* 51:717–728.
6. Rando RR (2001) The biochemistry of the visual cycle. *Chem Rev* 101:1881–1896.

7. Young RW, Bok D (1969) Participation of the retinal pigment epithelium in the rod outer segment renewal process. *J Cell Biol* 42:392–403.
8. Travis GH, Golczak M, Moise AR, Palczewski K (2007) Diseases caused by defects in the visual cycle: Retinoids as potential therapeutic agents. *Annu Rev Pharmacol Toxicol* 47:469–512.
9. Yang P, Tyrrell J, Han I, Jaffe GJ (2009) Expression and modulation of RPE cell membrane complement regulatory proteins. *Invest Ophthalmol Vis Sci* 50:3473–3481.
10. Sun H, Molday RS, Nathans J (1999) Retinal stimulates ATP hydrolysis by purified and reconstituted ABCR, the photoreceptor-specific ATP-binding cassette transporter responsible for Stargardt disease. *J Biol Chem* 274:8269–8281.
11. Weng J, et al. (1999) Insights into the function of Rim protein in photoreceptors and etiology of Stargardt's disease from the phenotype in abcr knockout mice. *Cell* 98:13–23.
12. Parish CA, Hashimoto M, Nakanishi K, Dillon J, Sparrow J (1998) Isolation and one-step preparation of A2E and iso-A2E, fluorophores from human retinal pigment epithelium. *Proc Natl Acad Sci USA* 95:14609–14613.
13. Wu Y, Fishkin NE, Pande A, Pande J, Sparrow JR (2009) Novel lipofuscin bisretinoids prominent in human retina and in a model of recessive Stargardt disease. *J Biol Chem* 284:20155–20166.
14. Sparrow JR, Yamamoto K (2012) The bisretinoids of RPE lipofuscin: A complex mixture. *Adv Exp Med Biol* 723:761–767.
15. Mata NL, Weng J, Travis GH (2000) Biosynthesis of a major lipofuscin fluorophore in mice and humans with ABCR-mediated retinal and macular degeneration. *Proc Natl Acad Sci USA* 97:7154–7159.
16. Radu RA, et al. (2008) Accelerated accumulation of lipofuscin pigments in the RPE of a mouse model for ABCA4-mediated retinal dystrophies following vitamin A supplementation. *Invest Ophthalmol Vis Sci* 49:3821–3829.
17. Schmitz-Valckenberg S, et al. (2008) Evaluation of autofluorescence imaging with the scanning laser ophthalmoscope and the fundus camera in age-related geographic atrophy. *Am J Ophthalmol* 146:183–192.
18. Sparrow JR, et al. (2010) Fundus autofluorescence and the bisretinoids of retina. *Photochem Photobiol Sci* 9:1480–1489.
19. Jayasundera T, et al. (2010) Peripapillary dark choroid ring as a helpful diagnostic sign in advanced Stargardt disease. *Am J Ophthalmol* 149:656–660 e652.
20. Sparrow JR, Nakanishi K, Parish CA (2000) The lipofuscin fluorophore A2E mediates blue light-induced damage to retinal pigmented epithelial cells. *Invest Ophthalmol Vis Sci* 41:1981–1989.
21. Finnemann SC, Leung LW, Rodriguez-Boulan E (2002) The lipofuscin component A2E selectively inhibits phagolysosomal degradation of photoreceptor phospholipid by the retinal pigment epithelium. *Proc Natl Acad Sci USA* 99:3842–3847.
22. Schütt F, Davies S, Kopitz J, Holz FG, Boulton ME (2000) Photodamage to human RPE cells by A2-E, a retinoid component of lipofuscin. *Invest Ophthalmol Vis Sci* 41:2303–2308.
23. De S, Sakmar TP (2002) Interaction of A2E with model membranes: Implications for the pathogenesis of age-related macular degeneration. *J Gen Physiol* 120:147–157.
24. Fishkin NE, Sparrow JR, Allikmets R, Nakanishi K (2005) Isolation and characterization of a retinal pigment epithelial cell fluorophore: An *all-trans*-retinal dimer conjugate. *Proc Natl Acad Sci USA* 102:7091–7096.
25. Zhou J, Kim SR, Westlund BS, Sparrow JR (2009) Complement activation by bisretinoid constituents of RPE lipofuscin. *Invest Ophthalmol Vis Sci* 50:1392–1399.
26. Zhou J, Jang YP, Kim SR, Sparrow JR (2006) Complement activation by photooxidation products of A2E, a lipofuscin constituent of the retinal pigment epithelium. *Proc Natl Acad Sci USA* 103:16182–16187.
27. Radu RA, et al. (2011) Complement system dysregulation and inflammation in the retinal pigment epithelium of a mouse model for Stargardt macular degeneration. *J Biol Chem* 286:18593–18601.
28. Radu RA, et al. (2005) Reductions in serum vitamin A arrest accumulation of toxic retinal fluorophores: A potential therapy for treatment of lipofuscin-based retinal diseases. *Invest Ophthalmol Vis Sci* 46:4393–4401.
29. Hageman GS, et al. (2001) An integrated hypothesis that considers drusen as biomarkers of immune-mediated processes at the RPE-Bruch's membrane interface in aging and age-related macular degeneration. *Prog Retin Eye Res* 20:705–732.
30. Hageman GS, et al. (2005) A common haplotype in the complement regulatory gene factor H (HF1/CFH) predisposes individuals to age-related macular degeneration. *Proc Natl Acad Sci USA* 102:7227–7232.
31. McHarg S, Clark SJ, Day AJ, Bishop PN (2015) Age-related macular degeneration and the role of the complement system. *Mol Immunol* 67:43–50.
32. Bora NS, Matta B, Lyzogubov VV, Bora PS (2015) Relationship between the complement system, risk factors and prediction models in age-related macular degeneration. *Mol Immunol* 63:176–183.
33. Mandal MN, Ayyagari R (2006) Complement factor H: Spatial and temporal expression and localization in the eye. *Invest Ophthalmol Vis Sci* 47:4091–4097.
34. Radu RA, Hu J, Jiang Z, Bok D (2014) Bisretinoid-mediated complement activation on retinal pigment epithelial cells is dependent on complement factor H haplotype. *J Biol Chem* 289:9113–9120.
35. Allikmets R, et al. (1997) Mutation of the Stargardt disease gene (ABCR) in age-related macular degeneration. *Science* 277:1805–1807.
36. Sweigard JH, Cashman SM, Kumar-Singh R (2011) Adenovirus-mediated delivery of CD46 attenuates the alternative complement pathway on RPE: Implications for age-related macular degeneration. *Gene Ther* 18:613–621.
37. Lyzogubov V, et al. (2014) Complement regulatory protein CD46 protects against choroidal neovascularization in mice. *Am J Pathol* 184:2537–2548.
38. Cashman SM, Ramo K, Kumar-Singh R (2011) A non–membrane-targeted human soluble CD59 attenuates choroidal neovascularization in a model of age-related macular degeneration. *PLoS One* 6:e19078.
39. Bora NS, et al. (2007) CD59, a complement regulatory protein, controls choroidal neovascularization in a mouse model of wet-type age-related macular degeneration. *J Immunol* 178:1783–1790.
40. Toops KA, Tan LX, Jiang Z, Radu RA, Lakkaraju A (2015) Cholesterol-mediated activation of acid sphingomyelinase disrupts autophagy in the retinal pigment epithelium. *Mol Biol Cell* 26:1–14.
41. Radu RA, et al. (2003) Treatment with isotretinoin inhibits lipofuscin accumulation in a mouse model of recessive Stargardt's macular degeneration. *Proc Natl Acad Sci USA* 100:4742–4747.
42. Miwa T, Song WC (2001) Membrane complement regulatory proteins: Insight from animal studies and relevance to human diseases. *Int Immunopharmacol* 1:445–459.
43. Vogt SD, et al. (2011) Retinal pigment epithelial expression of complement regulator CD46 is altered early in the course of geographic atrophy. *Exp Eye Res* 93:413–423.
44. Morgan BP (2016) The membrane attack complex as an inflammatory trigger. *Immunobiology* 221:747–751.
45. Lueck K, et al. (2011) Sub-lytic C5b-9 induces functional changes in retinal pigment epithelial cells consistent with age-related macular degeneration. *Eye (Lond)* 25:1074–1082.
46. Kunchithapautham K, Rohrer B (2011) Sublytic membrane-attack-complex (MAC) activation alters regulated rather than constitutive vascular endothelial growth factor (VEGF) secretion in retinal pigment epithelium monolayers. *J Biol Chem* 286:23717–23724.
47. Vogt SD, Barnum SR, Curcio CA, Read RW (2006) Distribution of complement anaphylatoxin receptors and membrane-bound regulators in normal human retina. *Exp Eye Res* 83:834–840.
48. Georgiannakis A, et al. (2015) Retinal pigment epithelial cells mitigate the effects of complement attack by endocytosis of C5b-9. *J Immunol* 195:3382–3389.
49. Sparrow JR, et al. (2013) Quantitative fundus autofluorescence in mice: Correlation with HPLC quantitation of RPE lipofuscin and measurement of retina outer nuclear layer thickness. *Invest Ophthalmol Vis Sci* 54:2812–2820.
50. Bavik C, et al. (2015) Visual cycle modulation as an approach toward preservation of retinal integrity. *PLoS One* 10:e0124940.
51. Fritsche LG, et al. (2012) A subgroup of age-related macular degeneration is associated with mono-allelic sequence variants in the ABCA4 gene. *Invest Ophthalmol Vis Sci* 53:2112–2118.
52. Maller JB, et al. (2007) Variation in complement factor 3 is associated with risk of age-related macular degeneration. *Nat Genet* 39:1200–1201.
53. Gold B, et al.; AMD Genetics Clinical Study Group (2006) Variation in factor B (BF) and complement component 2 (C2) genes is associated with age-related macular degeneration. *Nat Genet* 38:458–462.
54. Gehrs KM, Anderson DH, Johnson LV, Hageman GS (2006) Age-related macular degeneration: Emerging pathogenetic and therapeutic concepts. *Ann Med* 38:450–471.
55. Fritsche LG, et al. (2010) An imbalance of human complement regulatory proteins CFHR1, CFHR3 and factor H influences risk for age-related macular degeneration (AMD). *Hum Mol Genet* 19:4694–4704.
56. Foley S, Li B, Dehoff M, Molina H, Holers VM (1993) Mouse Crry/p65 is a regulator of the alternative pathway of complement activation. *Eur J Immunol* 23:1381–1384.
57. Lock M, et al. (2010) Rapid, simple, and versatile manufacturing of recombinant adeno-associated viral vectors at scale. *Hum Gene Ther* 21:1259–1271.
58. Radu RA, et al. (2008) Retinal pigment epithelium-retinal G protein receptor-opsin mediates light-dependent translocation of all-trans-retinyl esters for synthesis of visual chromophore in retinal pigment epithelial cells. *J Biol Chem* 283:19730–19738.
59. Hao W, Fong HK (1999) The endogenous chromophore of retinal G protein-coupled receptor opsin from the pigment epithelium. *J Biol Chem* 274:6085–6090.

Supporting Information

Lenis et al. 10.1073/pnas.1620299114

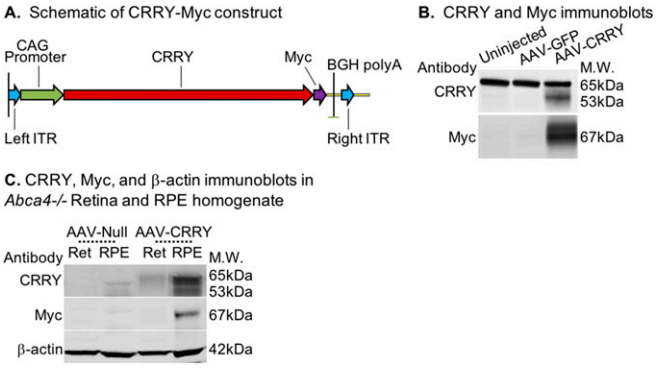

Fig. S1. AAV-CRRY construct to express an Myc-tagged CRRY protein delivered by subretinal injection. (*A*) Schematic of a CRRY-Myc construct delivered by subretinal injection. (*B*) Representative immunoblot of CRRY and Myc using RPE homogenate (40 μg protein per lane) from ∼2-mo-old mice. CRRY overexpression is evidenced by the 53-kDa isoform at 5 wk after subretinal injection of 0.5 μL of AAV-CRRY virus; Myc staining is seen only in the AAV-CRRY sample. (*C*) Representative immunoblot of CRRY, Myc, and β-actin using retina (Ret) and RPE homogenates from ∼3-mo-old *Abca4*$^{-/-}$–injected mice (30 μg protein per lane). At 9 wk after subretinal injection of 0.5 μL of AAV-CRRY virus, both 53- and 65-kDa CRRY isoforms are overexpressed in the AAV-CRRY samples. Note that Myc immunoreactivity is seen only in RPE of the mice injected with AAV-CRRY virus. Moreover, the retina homogenates do not show any detectable Myc immunoreactivity.

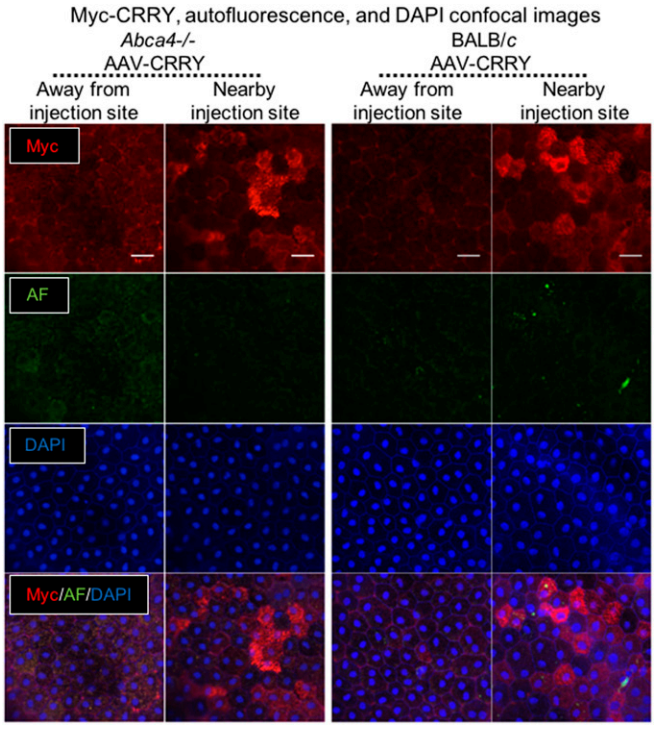

Fig. S2. RPE autofluorescence pattern and CRRY-Myc staining in CRRY-injected *Abca4*$^{-/-}$ and BALB/*c* mice. Representative confocal images of Myc (red) and DAPI (blue) immunohistochemistry; autofluorescence (AF; green) acquired at 488-nm excitation wavelength of 6-mo-old AAV-CRRY–injected *Abca4*$^{-/-}$ mice (*Left*) and BALB/*c* mice (*Right*). Note increased Myc immunostaining of RPE cells in the area near the injection site, corresponding to the superior-temporal quadrant. In contrast, there is significantly reduced Myc immunostaining of RPE cells in the area away from the injection site, corresponding to the inferior-nasal quadrant. Autofluorescence (green) distribution is inversely related to Myc immunoreactivity in the *Abca4*$^{-/-}$ mice, unlike the BALB/*c* mice, which show negligible RPE autofluorescence. (Scale bars: 20 μm.)

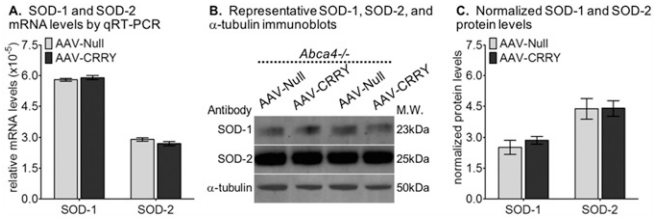

Fig. S3. AAV-CRRY treatment does not change the oxidative stress level in *Abca4*$^{-/-}$ mice. (*A*) Histogram showing the relative SOD-1 and SOD-2 mRNA levels by qRT-PCR. Each mRNA level was normalized to 18S rRNA. (*B*) Representative immunoblots of SOD-1, SOD-2, and α-tubulin using RPE homogenate (10 μg of protein per lane). (*C*) Histogram showing SOD-1 and SOD-2 normalized protein data in the RPE homogenate samples shown in *B*. Protein and cDNA samples were obtained from 7-mo-old *Abca4*$^{-/-}$ mice injected with AAV-CRRY and -null viruses ($n = 4$). Each protein and cDNA sample was run in triplicate.

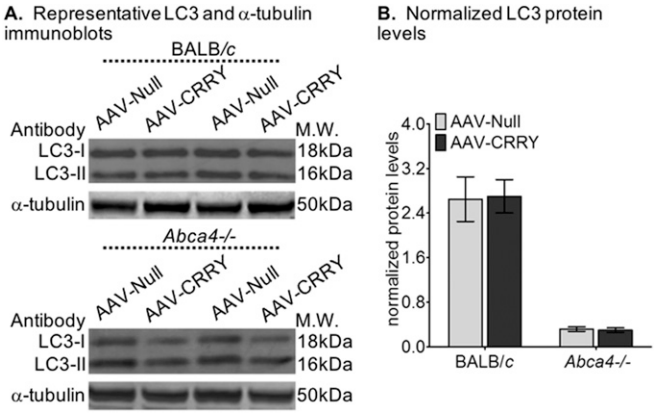

Fig. S4. LC3 activity in the RPE of *Abca4*$^{-/-}$ mice is not affected by the AAV-CRRY treatment. (*A*) Representative immunoblots of LC3 and α-tubulin using RPE homogenate (10 μg protein per lane) of BALB/*c* (*Top*) and *Abca4*$^{-/-}$ (*Bottom*). (*B*) Histogram showing LC3 normalized protein data in the RPE homogenate samples shown in *A*. RPE protein samples were obtained from 7-mo-old mice injected with AAV-CRRY and -null viruses ($n = 4$). Each protein sample was run in triplicate.